Closed-loop buoyancy control for a Coastal Profiling Float

Laughlin Barker, Santa Clara University

Mentor: Gene Massion

Summer 2014

Keywords: profiling float, buoyancy engine, control, PID, root locus, linearization

ABSTRACT

A closed-loop velocity-position cascade control system for a profiling float is investigated, simulated, and tested. In the dynamic model, drag experienced by the plant is linearized to facilitate Laplace Transform, and transfer function is computed. A discrete-time PID controller with low-pass signal filter is integrated into the model in the Laplace domain, and resulting Root Locus computed. For a tested set of control gains the Root Locus predicts an over damped response to step input. Simulink simulation of the non-linear plant, and subsequent testing in the MBARI Test Tank showed the plant exhibited slight oscillation when given a step input. The cascaded strategy was successful in depth control within +/- 0.2 dbar, but is energetically expensive. For long term float deployments, a more efficient strategy of achieving neutral buoyancy is needed.

NOMENCLATURE

F_B	Buoyant Force [N]	C_D	Drag Coefficient
F_G	Gravitational Force [N]	A	Float Frontal Area [m^2]
F_D	Drag Force [N]	g	Gravitational Acceleration, -9.81 m/s^2
V	Instantaneous Float Volume [m^3]	c_{lin}	Velocity linearization parameter
V_0	Static Float Volume [m^3]	a, b	Transfer Function Coefficients
$\dot{V}$	Buoyancy Engine Flow Rate [m^3/s]	u	Control Signal
m	Float Mass [kg]	V_{SP}	Velocity Set Point [m/s]
$\dot{z}$	Velocity [m/s]	IB, OB	Velocity Control Bands [m]
ρ_{sw}	Sea Water Density [kg/m^3]		

INTRODUCTION

Coastal waters (defined by the continental shelf), are highly productive environments. While occupying only 7-10% of total ocean area, it is estimated they are responsible for 40-50% of net primary productivity in the ocean (Bauer et al. 2013, Ducklow & McCallister 2004). In a study of oceanic and terrestrial systems, Geider et al (2001) estimate that globally, coastal waters are responsible for approximately 10% of the Earthôs net primary productivity.

While undoubtedly important, a lack of appropriate temporally and spatially scaled data has left our understanding of these systems with a high degree of uncertainty (Bauer et al. 2013). High cost has prevented historical biogeochemical studies (research cruises) from being scaled to capture the heterogeneous nature of these waters. In the last ten years however, low-power biogeochemical sensors (pH, Oxygen, Nitrate, pCO_2 and others), have been developed and are being proven to be suitable for long-term observation systems (Johnson et al 2009). With the advent of these sensors, the primary technical challenge of implementing a coastal observing network lies in cost effective long-term deployment of these sensors.

Perhaps the single tenable option for a scalable coastal biogeochemical observing network is through the use of profiling floats. The Argo Array, launched in 1999 currently sports over 3,600 Apex Profiling Floats which profile the top 2,000 m of the worldôs oceans (on average) every 10 days. The profilers have a battery life of 4-5 years, and telemeter collected data via satellite during surface intervals. The life-cycle cost,

including Iridium/Argo satellite fees, of a single Apex float is approximately $30,000 (Argo FAQ).

While the underlying technology of profiling floats has been successfully scaled to a global deployment, several challenges of working in shallow coastal waters preclude the use of commercially available profilers in coastal environments. Figures 1 (a) and (b) show the trajectory and maximum depth of an Apex float operating in the Pacific Ocean. Excessive drift and coarse depth control make operating these floats in small and shallow (< 500 m) measurement volumes difficult.

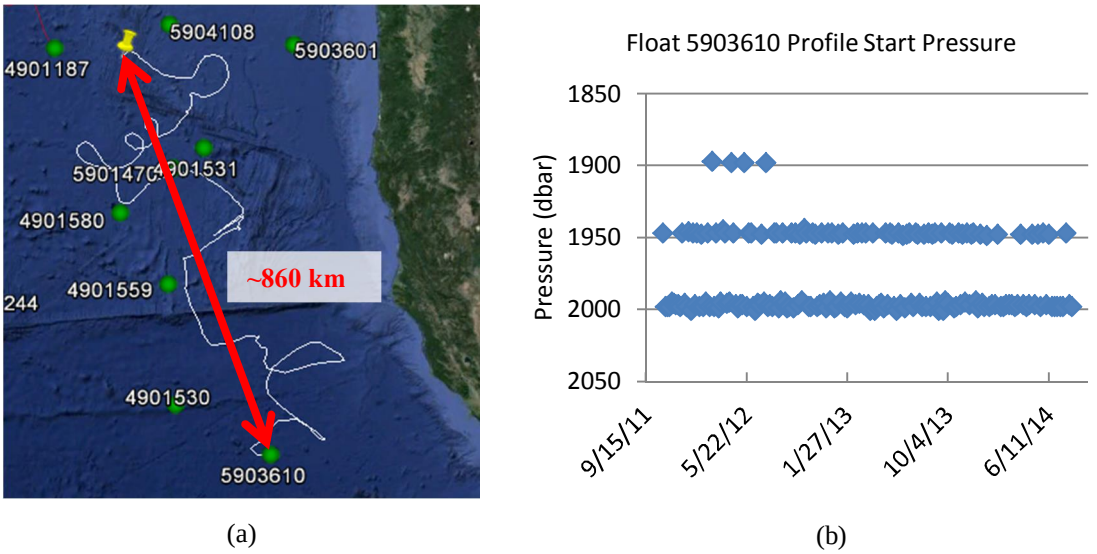

(a) (b)

Figure 1: Apex (Argo) profiling floats often exhibit large drift and coarse depth control, making them unsuitable for operation in coastal waters (which are small and shallow by nature). The 1,016 day trajectory of a single float can be followed with the white line in (a). The start pressure of each profile is shown in (b) and shows the coarse nature of the floatôs depth control.

To address these challenges, in 2012 the MBARI Chemical Sensors Laboratory began development of the Coastal Profiling Float (CPF). To minimize drift, the CPF is designed to ñanchorò itself by becoming negatively buoyant and resting on the benthos between profiles. Closed-loop buoyancy control will ensure accurate platform velocity and depth control should the float park itself in the midwater.

MATERIALS AND METHODS

CONTROL STRATEGY

Because control of both velocity and position of the CPF are desired, it was decided to design and implement a cascaded velocity-position controller. By designing a velocity profile with respect to displacement from a desired position, cascaded control strategies allow one to control a plantôs velocity and position. Such controllers are commonly used in industrial CNC machine tools (Karlsson 2009 & Mandra 2014). In Figure 2, the general structure of the closed-loop control system for the CPF is shown. The target depth, velocity set point, controller, control signal, plant model, and depth are represented by, *r, Vsp,* $G_c(s)$*,u,* $G_p(s)$*,* and *z* respectively.

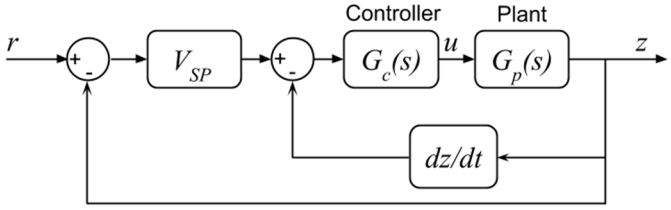

Figure 2: To control the CPF, a cascaded velocity-position controller is used. Position of the float relative to its target depth, *r*, adjusts the velocity set point according to a table in V_{SP}. To control velocity, a PID controller acts on discrete (and filtered) differentiation of pressure samples.

PLANT MODEL

To design a closed-loop controller, it is first necessary to model the dynamics of the plant of interest. Figure 3 shows the free body diagram of a profiling float during ascension.

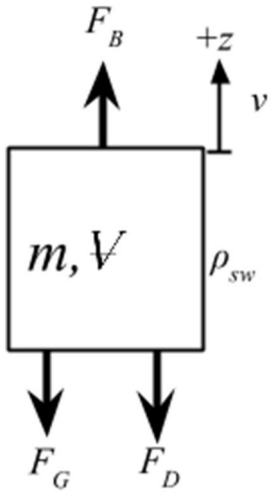

Figure 3: To model system dynamics, a free body diagram is drawn with relevant forces that act on the system: buoyancy, gravity, and drag, labeled F_B, F_G, and F_D respectively. Additionally, the body has some mass, m, volume, $\forall$, and velocity, v.

The float has some mass, m, volume, $\forall$, velocity, v, and the seawater having some density, ρ_{sw}. The buoyant, drag, and gravitational forces are given by:

$$F_B = \underbrace{\forall_0 \rho_{sw}|g|}_{constant} + \underbrace{\rho_{sw}|g| \int_0^t \dot{\forall}(\tau)d\tau}_{variable} \tag{1}$$

$$F_D = -\frac{1}{2}\rho_{sw} C_D A v|v| \tag{2}$$

$$F_G = -mg \tag{3}$$

where $\forall_0$ and $\dot{\forall}(t)$ are the floatôs fixed volume, and buoyancy engineôs volumetric flow rate respectively. The buoyancy engineôs flow rate is chosen as the control variable because it is proportional to the rotational speed of the motor driving the pump and thus easily controlled. The velocity component of the drag term is given by $v|v|$ and not v^2 so the sign of v is respected. The buoyancy term can be simplified and gravitational term eliminated by assuming the constant buoyant force is equal to the gravitational force of the float. The simplified equation of motion is then given by,

$$\sum F = m\dot{v} = \rho_{sw}|g| \int_0^t \dot{\forall}(\tau)d\tau - \frac{1}{2}\rho_{sw} C_D A v|v| \tag{4}$$

This equation of motion is used as the basis for a full dynamic simulation in MATLAB Simulink. As implemented, the model includes features such as: realistic sea water density profiles computed from MBARI ROV Ventana CTD data, added mass factor, pump (in)efficiency, ideal-gas law compressibility to model air trapped in the buoyancy engine, and the linear drag experienced by an object moving slowly (Re < 100) through a stratified fluid as described by DôAssaro (2003).

For development of a controller however, the equation of motion is used without the above mentioned complexities, and drag term linearized to allow representation in the Laplace Domain. Drag is linearized such that the linear approximation, $\hat{F}_D$, yields an equal drag force at zero velocity, and some nominal velocity, v_{nom},

$$\hat{F}_D = F_D|_{v=v_{nom}}$$

$$-\frac{1}{2}\rho_{sw} C_D A v_{nom} c_{lin} = -\frac{1}{2}\rho_{sw} C_D A v_{nom} |v_{nom}|$$

$$c_{lin} = |v_{nom}|$$

$$\hat{F}_D = -\frac{1}{2}\rho_{sw} C_D A c_{lin} v \tag{5}$$

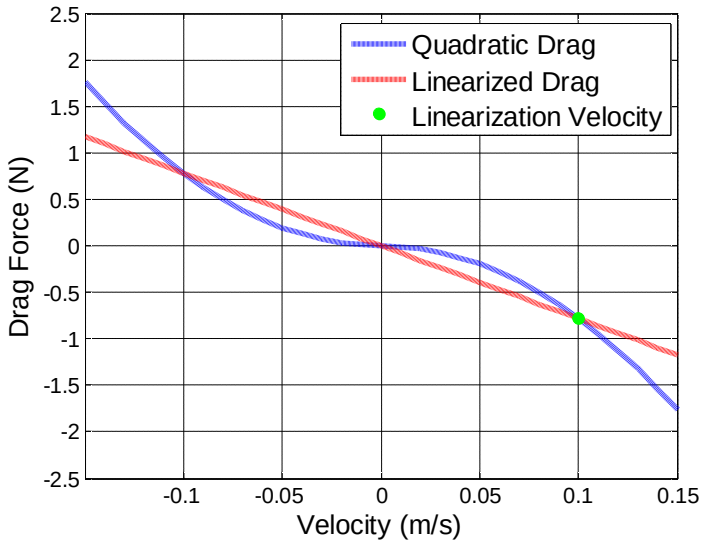

Figure 4: To perform a Laplace transform on the equation of motion, the non-linear drag term is linearized at the zero velocity point, and some nominal platform velocity, v_{nom}, shown here as 0.1 m/s. The quadratic drag shown here was computed with ρ_{sw} = 1027 kg/m^3, C_D = 1.5, and A = 0.1018 m^2.

By grouping terms,

$$a = \rho_{sw}|g|\,, \quad b = \frac{1}{2}\rho_{sw}C_D A c_{lin}$$

the linearized equation of motion is transformed into the Laplace domain, and open-loop transfer function, $G_p(s)$, found,

$$m\dot{v} = a\int_0^t \dot{\Psi}(\tau)d\tau - bv \tag{6}$$

$$mV(s)s = a\frac{\dot{\Psi}(s)}{s} - bV(s) \tag{7}$$

$$G_p(s) = \frac{V(s)}{\dot{\Psi}(s)} = \frac{a}{s(ms+b)} \tag{8}$$

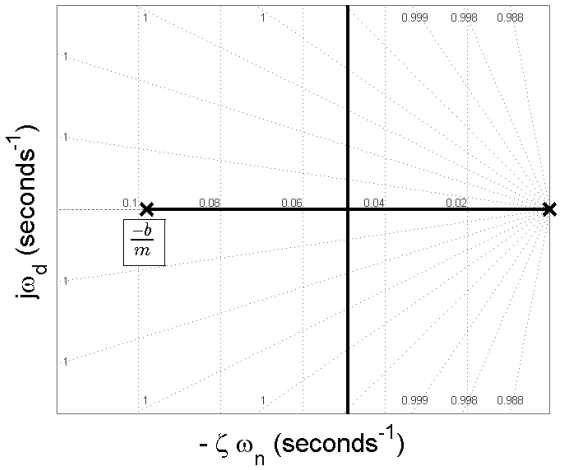

Figure 5: The open loop transfer function given by Equation 8 has two poles, located at $s = 0$ and $-b/m$.

TEST TANK PROTOTYPE

A Test Tank Prototype (TTP) of the CPF was built in early 2012 as a proof of concept, and served as the test platform for the development of the controller. Figures 6 (a) shows the prototype, with relevant system components listed in 6 (b).

(a)

Element	Value/Description
m	38 kg
Adjustable Buoyancy	3 L
Power	Qty 6: Tenergy Li-Ion 25.9V 2600mAh Batteries
Micro Controller	EMX System on Module (.NET Micro Framework w/C#)
Motor	Maxon RE65 w/Quadrature Encoder
Motor Controller	Elmo Solo Whistle
Pump	Oildyne 692
Pressure Transducer	Honeywell 20psi 4-20mA
Pressure Transmitter	Omega DGH D1000 Series 4-20mA A/D

(b)

Figure 6: The Test Tank Prototype used during testing of the control system was built in 2012 and is shown in (a). Relevant power, control, and platform parameters are listed in the table shown in (b).

CONTROLLER

A discrete PID controller with second-order low-pass filter had been previously implemented in on the CPFôs microcontroller by Gene Massion. The controller and filter is based on a discrete-time controller found in Åström and Hägglund (2006). In its continuous form, the controller is modeled by,

$$u(t) = K\left(y_{sp} - y_f + \frac{1}{T_i}\int_0^t \left(y_{sp}(\tau) - y_f(\tau)\right)d\tau + T_d\frac{dy_f(t)}{dt}\right) \tag{9}$$

The filtered input signal, y_f is produced by a second-order low-pass filter (LPF), which is also implemented in the algorithm. The transfer function of this filter is,

$$\frac{Y_f(s)}{Y(s)} = \frac{1}{1 + sT_f + \frac{(sT_f)^2}{2}} \tag{10}$$

where T_f is the time constant of the filter. This filter has a damping coefficient of 0.707, corresponding to ~4.3% overshoot. A low-pass filter of sufficiently low cut off frequency

has the ability to filter not only the electrical noise that may be present on the pressure transducer line, but also sinusoidal pressure signals resulting from wave action when the float is near the surface. It is desirable to filter out these low-frequency wave signals as acting upon them would be a poor use of the floatôs limited energy budget. Figure 7 shows a spectrogram of wave height for different wind speeds in fully develop seas. Based on this graph, it was decided that a 3 dB cut off frequency of 0.1 Hz (T_f = 1.59) would minimize influence to the system by smaller waves, without introducing excessive error signal delay into the system. Here, excessive time delay is defined as a rise time approximately equal to, or larger than, the open-loop response of the system to a step input. The settling time, T_s, for the 0.1 Hz LPF filter is approximately 9.6 seconds.

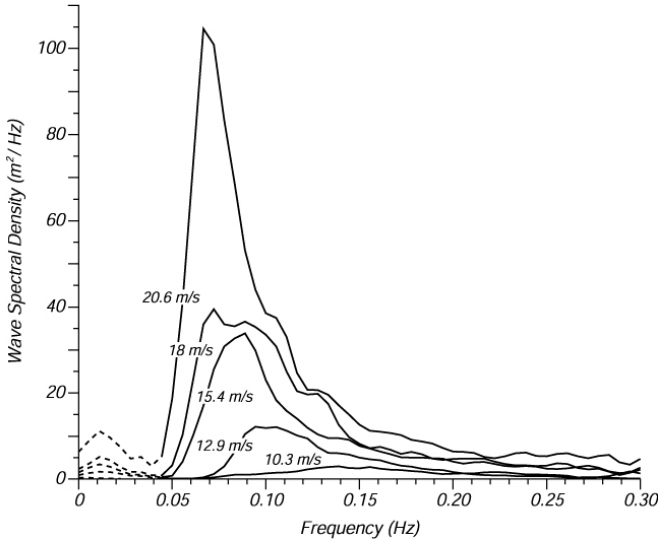

Figure 7: Wave frequency varies with amplitude, which is influenced by wind speed. Plotted here is the wave spectrogram for different wind speeds in fully developed seas. A 3 dB low-pass frequency of 0.1Hz was chosen and implemented in the filter. Figure from Moskowitz (1964).

The overall transfer function of the PID controller and second order filter, $G_c(s)$, is given by,

$$G_c(s) = K\frac{(s+z_1)(s+z_2)}{s\left(1+sT_f+\frac{(sT_f)^2}{2}\right)} \tag{11}$$

For Root Locus analysis & modeling, the plant transfer function was imported into the MATLAB `sisotool`. Complex poles representing the filter were added, an integration pole, and the two zeros were added.

As a starting point, existing hand-tuned gain values (K = 70, T_D = 10, T_I = 50,000) were used in the velocity controller. Previous modeling indicated the controller was stable (likely over damped), and achieved a settling time of ~90 s ï relatively slow in the context of many dynamic mechanical systems, but acceptable for a profiling float in the ocean.

The velocity set point table is broken into three bands: mission velocity, approach velocity, and zero velocity. Mission velocity is the primary velocity at which the float ascends or descends between waypoints. Approach velocity is a small velocity to help ñguideò the float to the appropriate depth, (and return it to that depth should it leave the park area unexpectedly), and, as expected, zero velocity is a set point of 0 m/s.

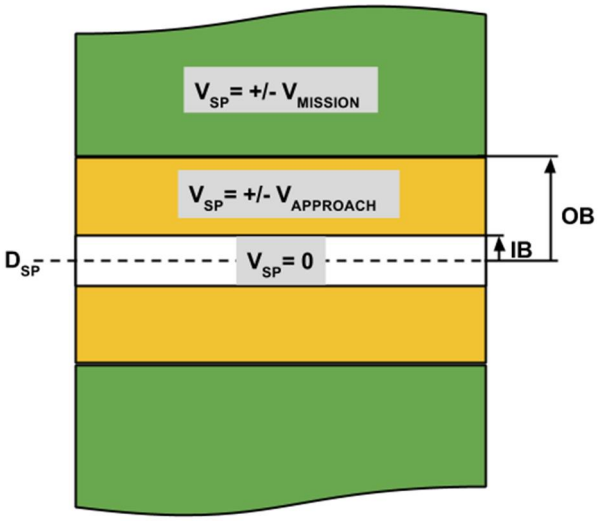

Figure 8: The velocity set point controller for the CPF is discrete instead of continuous. When the float is far away (> *OB* m) from its depth set point, the mission-defined velocity is the velocity set point. Once the float is inside the yellow band, bounded by *IB* and *OB,* the set point velocity is adjusted to the approach velocity, 0.01 m/s. Finally, once the float enters the park depth, D_{SP}+/- *IB*, velocity is set to zero. This approach allows for some settling and provides a dead band to prevent oscillation when in the park zone. Should the float drift out of the park zone however, it will be commanded back with a slow velocity ñnudgeò to put it back inside.

RESULTS

SIMULATION

The simulation was run with the added mass factor (25%) and $C_D = 1.5$ found by Sohn (2013). Simulation results show the controller should be capable of achieving zero velocity, meaning the float should be capable of non-oscillatory depth holding. Placing zeros at the locations corresponding to the PID gains mentioned above and plotting the Root Locus, via `sisotool`, one can examine the predicted model response over a range of gains,

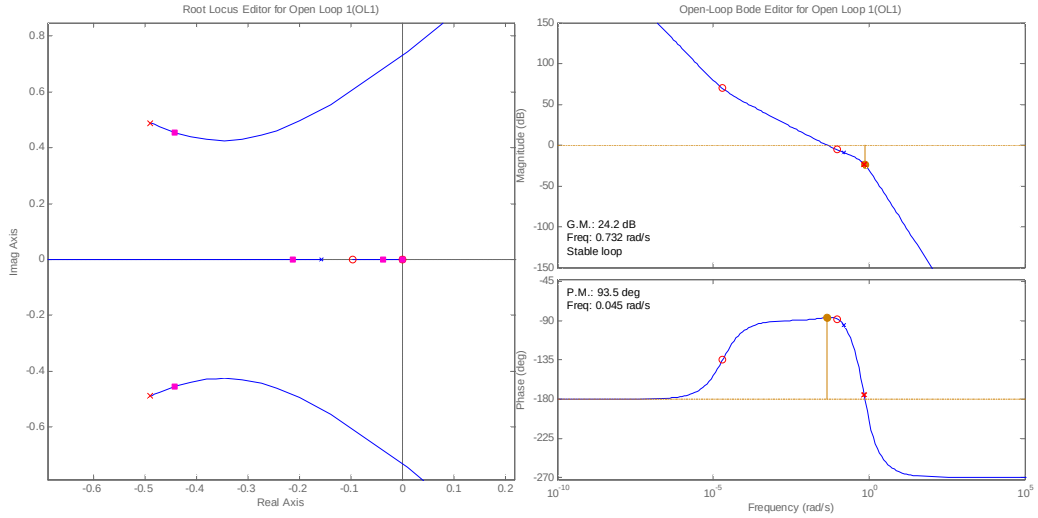

Figure 9: The MATLAB `sisotool` produced Root Locus and Bode responses for the closed loop velocity controller. Dominant (slow, or close to the imaginary axis) poles have no complex component, so no oscillation is expected when the system is given a step input. For a controller gain of ~700, the poles are shown in pink. Gain and Phase margins of 24 and 93 dB respectively indicate the controller is stable given the physical parameters of the plant, and that there is room for some amount of gain increase, plant model uncertainty, and/or even higher drive frequency.

Platform response to velocity input signal was good, though difficult to measure. Sample time for the controller and pressure transducer was set to 1s, and the 4-20 mA to RS-232 converter provided approximately 0.065 dbar (~6.5 cm) resolution. Discrete pressure samples were put through a differentiator filter, which in turn estimated velocity. Figure 10 shows the command and response of the system to the velocity set point over the course of a dive.

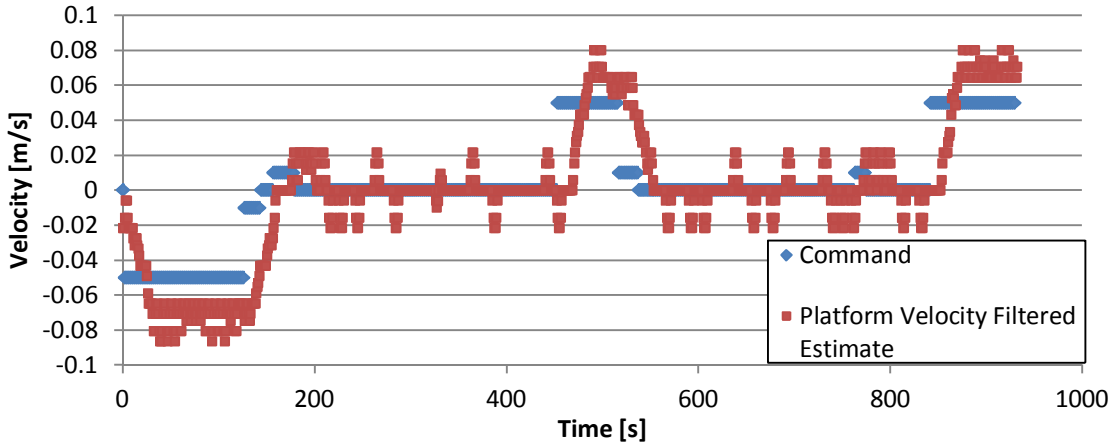

Figure 10: Blue lines show commanded velocity over the course of a dive profile, while red shows the differentiator filter estimation of velocity. Because pressure samples were taken at 1Hz, and the pressure sensors & A/D combination had a resolution of 0.065 m, sequential pressure measurements could only provide coarse velocity measurements. It is worthy to note that when commanded to maintain zero velocity, the platform appears to show slight oscillatory behavior about 0 m/s.

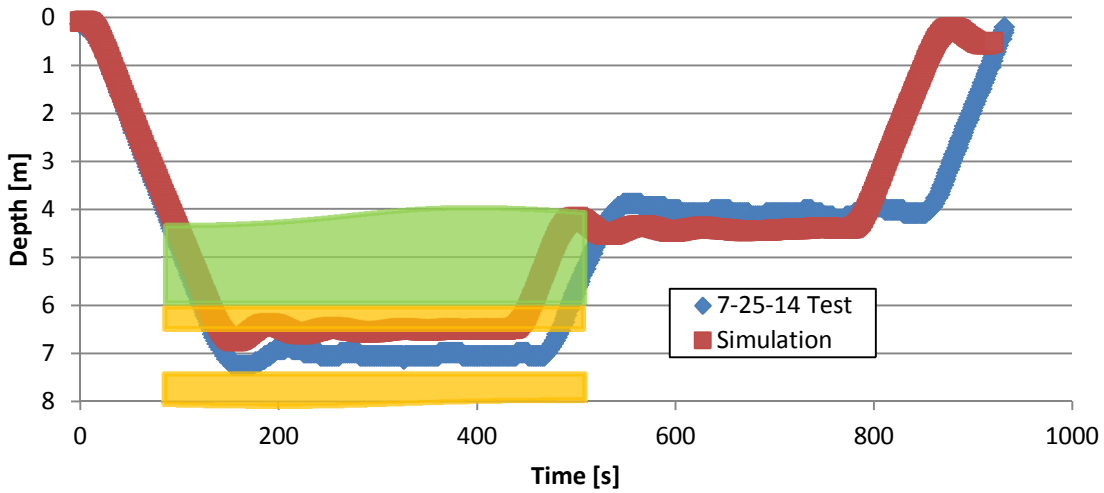

Figure 11: The depth profile of a dive to 7 and 4 m, with two 300 s holds is shown. The commanded descent and ascent velocity was 0.05 m/s, with *IB* = 0.2 m and *OB* = 1 m. Both the simulation and test showed slight oscillatory motion when trying to hold zero velocity. Once settled, the float does not leave the +/- 0.2 m band. While depth deviations are small, their presence is easily detected examining the velocity measurements of the float (Figure 10). The superimposed yellow and green bars depict the approximate velocity set point thresholds as shown in Figure 8.

DISCUSSION

The Root Locus plot predicts an over-damped, and thus non-oscillating response to a step input of 0.05 m/s to the velocity controller. It should be remembered that this response is based on a linear approximation of the decidedly non-linear plant. Considering this fact,

the presence of slight oscillations while trying to hold zero velocity is not surprising. Intuitively, this makes sense as the slope of the drag curve in the linearized model is constant, whereas it approaches zero in for the quadratic drag regime, meaning that for a given change in velocity near 0 m/s, the expected change in drag is quite different between the linear and non-linear systems.

The cascaded position strategy is effective at holding depth, as can be seen in Figure 11. This process is active however, as the motor is constantly making adjustments, and based on the velocity profile in Figure 10, oscillating. While successful at holding position, this is energetically expensive, and is thus not suitable for a long term deployment.

CONCLUSIONS

A cascaded velocity-position controller was analyzed, implemented, and tested on a prototype of the MBARI Coastal Profiling Float. The approach uses a discrete PID implementation with second-order low-pass filter described by Åström and Hägglund (2006). A velocity set point table uses depth error to adjust the velocity set to achieve desired depth.

The cascaded strategy is shown to be successful in controlling velocity and position. Slight oscillatory motion is observed when the float is near zero velocity, possibly due to the difference between the linearized float model, and the non-linear drag experienced by the float.

A neutral buoyancy routine should be investigated and implemented in order to make the float energetically efficient during mid-water park periods.

ACKNOWLEDGEMENTS

I would like to thank Gene Massion for his guidance over the course of this internship. His years of experience and breadth of knowledge in the field of ocean engineering combined with his light hearted nature make him one of the most enjoyable and accessible experts in the field. I also thank Wayne Radochonski, for helping me through C# - I would have been stuck writing RS-232 drivers for several weeks without his help. I also thank Paul Coenen, Jonny Ferreira and Jim Montgomery for their help with all things mechanical and electrical on the tank prototype. To Ken Johnson and the rest of the Chemical Sensors Lab: thank you for welcoming me into your lab; you are doing

some truly exciting things! To George Matsumoto and Linda Kuhnz, I wouldnôt have had this opportunity were it not for your vision and dedication to the internship program, thank you! Finally I extend my thanks to all the other MBARI staff, adjunct faculty, and last but certainly not least, the David and Lucile Packard Foundation.

References:

Argo FAQ. Accessed: 9 August 2014. http://www.argo.ucsd.edu/FAQ.html

Åström, K.J., and T. Hägglund (2006). Advanced PID Control, Instrumentation, Systems, and Automation Society.

Bauer, J. E., W-J. Cai, P.A. Raymond, T.S. Bianchi, C.S. Hopkinson, and P.A.G. Regnier (2013). The changing carbon cycles of the coastal ocean. *Nature,* **504**: 61-70.

DôAssaro, E.A. (2003). Performance of autonomous lagrangian floats. *J. Atmospheric and Oceanic Technology,* **20**: 896-911.

Ducklow, H.W. and S. L. McCallister (2005). The Biogeochemistry of carbon dioxide in the coastal oceans, *The Sea*, **13**: 269-315.

Geider, R.J., E.H. Delucia, P.G. Falkowski, A.C. Finzi, J.P. Grime, J. Grace, T.M. Kana, J. La Rouche, S.P. Long, B.A. Osborne, T. Platt, I.C. Prentice, J.A. Raven, W.H. Schlesinger, V. Smetacek, V. Stuart, S. Sathyendranath, R.B. Thomas, T.C. Vogelmann, P. Williams, F.I. Woodward (2001). Primary productivity of planet earth: biological determinants and physical constraints in terrestrial and aquatic habitats. *Global Change Biology,* **7**: 849-882.

Johnson, K.S**.**, W.M. Berelson, E.S. Boss, Z. Chase, H. Claustre, S.R. Emerson, N. Gruber, A. Körtzinger, M.J. Perry, and S.C. Riser (2009). Observing biogeochemical cycles at global scales with profiling floats and gliders: Prospects for global array. *Oceanography,* **22**: 216-225.

Moskowitz, L. (1964). Estimates of the power spectrums for fully developed seas for wind speeds of 20 to 40 knots, *J. Geophysical Research*, **69**: 5161ï 5179.

Shon, C. (2013). Developing parameter estimation techniques for controller optimization of a Coastal Profiling Float, *MBARI Intern Report*.